Materials and Design 31 (2010) 4836–4841

Contents lists available at ScienceDirect

Materials and Design

journal homepage: www.elsevier.com/locate/matdes

Short Communication

Study on microstructure of low carbon 12% chromium stainless steel in high temperature heat-affected zone

Huaibei Zheng [a,b,*], Xiaoning Ye [b], Laizhu Jiang [a,b], Baosen Wang [b], Zhenyu Liu [a], Guodong Wang [a]

[a] The State Key Laboratory of Rolling and Automation, Northeastern University, Shenyang 110004, China
[b] Research Institute, Baoshan Iron & Steel Co., Ltd., Shanghai 200431, China

ARTICLE INFO

Article history:
Received 21 March 2010
Accepted 28 May 2010
Available online 2 June 2010

ABSTRACT

Coarsening, embrittlement and corrosion sensitization in high temperature heat-affected zone (HTHAZ) are the major problems when low carbon 12% chromium stainless steel is being welded, which induce deterioration of the impact toughness at low temperature and intergranular corrosion resistance. This study investigated the corresponding microstructures in HTHAZ with different chemical compositions and heat inputs through thermal simulation tests. There are several primary conclusions: (1) When ferrite factor (FF) is above 9.0, the microstructure in HTHAZ is fully ferrite or a small amount of martensite net likely distributing along delta ferrite grain boundaries. On the other hand, if FF is below 9.0, the martensite content increases with the decreasing of FF. (2) Heat input influences the microstructure of high FF steel in HTHAZ. The martensite content and its distribution of low FF steel are not sensitive to heat inputs, but the grain size grows up with the increase of heat inputs. (3) The coarse Ti-rich particles in low FF steels containing Ti can promote intragranular austenite formation inside delta ferrite resulting in packet morphology of martensite. On the other hand, martensite of low FF steels only stabilized with Nb is characterized by grain boundary allotriomorphs, Widmanstätten structures and secondary sawteeth. This martensite reticularly distributes along ferrite grain boundaries.

1. Introduction

Comparing with carbon steels and weathering steels, low carbon 12% chromium stainless steel has good corrosion resistance. Although it has higher initial costs compared to carbon steels, low chromium stainless steel provides lower total life costs due to longer life with less coating renewals and lower maintenance, which shows significantly economic and environmental advantages. 3CR12 stainless steel is known as the first generation of these steels which conform to grades UNS41003 [1] and 1.4003 [2,3], respectively, in ASTM A240, EN 10088-2 and EN 10028-7. It provides an alternative which displays both the advantages of stainless steels and engineering properties of carbon steel [4–6]. There are several steels such as Nirosta 4003 supplied by ThyssenKrupp Nirosta, 41003 and 409Ni produced by AK Steel, as well as 5CR12Ti developed by Sandvik [7–10]. In recent years, TCS345 and T4003 have been developed by steel manufacturers in China for the application of ferritic stainless steel in rail wagons [11], and the JFE has also developed 410RW to meet customers' demand [12]. The applications of these steels include rail transport, road transport, materials handling, petrochemicals and chemicals, power generation, water and sewage treatment, telecommunication cabinets and electrical enclosures [6–10].

The Fe–Cr equilibrium phase diagram is shown in Fig. 1, and the contents of other elements are 0.015%C, 0.01%N, 0.3%Si, 1.5%Mn and 1.0%Ni. The phase diagram of 12%Cr stainless steel is divided into several fields: single delta ferrite phase field, delta ferrite and austenite dual phase field, and single austenite phase field. The dual phase field and single austenite phase field extend with decreasing of the Cr content, while the range of single delta ferrite phase field reduces and the transformation temperature of delta ferrite to austenite tends to be higher. The austenite appearing at high temperature effectively restricts the grain growth in HTHAZ. Consequently, the weldability, especially the as-welded toughness of these steels, is improved [13].

Mechanical properties and corrosion sensitization of welded joints of these steels have been widely studied [4,12–18]. Based on their studies, coarsening, embrittlement and corrosion sensitization in high temperature heat-affected zone (HTHAZ) are the major problems when low carbon 12% chromium stainless steel is being welded, which result in deterioration of the impact toughness at low temperature and intergranular corrosion resistance. Therefore, this study focuses on the microstructures in HTHAZ with different chemical compositions and heat inputs.

* Corresponding author at: The State Key Laboratory of Rolling and Automation, Northeastern University, Shenyang 110004, China. Tel.: +86 21 26034484; fax: +86 21 26034622.
E-mail address: zhb021233@yahoo.cn (H. Zheng).

0261-3069/$ - see front matter Crown Copyright © 2010 Published by Elsevier Ltd. All rights reserved.
doi:10.1016/j.matdes.2010.05.054

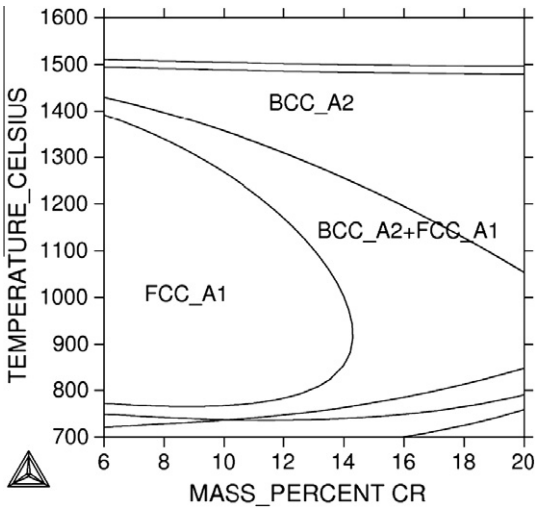

Fig. 1. Fe–Cr equilibrium phase diagram. (The other elements are 0.015%C, 0.01%N, 0.3%Si, 1.5%Mn and 1.0%Ni.)

2. Experimental procedure

Chemical compositions of the steels used are given in Table 1. The ferrite factors (FF) are calculated from the following equation [18]:

$$FF = Cr + 6Si + 8Ti + 4Mo + 2Al + 4Nb - 2Mn - 4Ni - 40(C + N). \quad (1)$$

The tested steels were hot rolled into 6 mm thick plate, followed by annealing at 993 K for 4 h. Welding thermal cycles of different heat inputs in HTHAZ were reproduced with Gleeble 3800 which is one of the best thermo-mechanical simulators developed by Dynamic Systems Inc. Parameters of the welding thermal cycles are shown in Table 2. Specimen size is 5 mm(thickness) × 10 mm(width) × 55 mm(length). Tested steels B, C, D and H were welded by gas metal arc welding (GMAW) in order to compare them with the thermal simulation test results. Welding conditions are shown in Table 3.

Microstructures were observed with an optical microscope. The percentage of martensite was measured with the image processing software Photoshop 8.0. At first, the ferrite in one photo was selected, and the corresponding pixels were counted. After the total pixels of the picture were measured, the pixels of martensite could be simply obtained by subtracting the pixels of ferrite from the pixels of the picture. Finally, the proportion of martensite was calculated through dividing the pixels of the picture by those of the martensite.

3. Results

Martensite contents of these steels in HTHAZ at different heat inputs are shown in Table 4. Fig. 2 shows a comparison of the results of the thermal simulation of B, C, D and H at the heat inputs of 0.5 kJ/mm and 0.7 kJ/mm with the GMAW results at the heat input of 0.6 kJ/mm. The thermal simulation results are consistent with welding results; accordingly, the results of thermal simulation tests are reliable.

3.1. Martensite content

The microstructure of higher FF steels in HTHAZ with very low heat inputs is almost fully ferrite, as shown in Fig. 3a the microstructure of steel L whose FF equals to 9.71 at the heat input of 0.3 kJ/mm. Fig. 3b shows the microstructure of steel L at the highest heat input of 1.5 kJ/mm, and it consists of coarse delta ferrite and a little martensite located at ferrite grain boundaries. According to Table 4, when the FF is above 9.0, the martensite content obviously increases with heat inputs.

Fig. 4 shows the microstructure of steel C whose FF is 8.02. Microstructure of low FF steel in HTHAZ consists mostly of martensite at different heat inputs. When the FF is below 8.24, the percentage of martensite at different heat inputs is higher than 90%. Heat inputs have a weak effect on the martensite content and its distribution of low FF steel in HTHAZ, but the grains grow up with an increase of heat inputs. However, the proportion of martensite in the steels, in which the FF is range from 8.35 to 8.8, rapidly increases with heat inputs. The FF of steels F and G with Nb stabilization are lower than steel H with Ti stabilization; however, its martensite content is less than that of steel H.

3.2. Martensite distribution and morphology

When the percentage of martensite is lower, the martensite net likely distributes along delta ferrite grain boundaries as shown in Figs. 3b and 5a. In these two pictures, grain boundary allotriomorphs are obviously observed. Secondary sawteeth and sideplates are also found to grow from the allotriomorph structure. These martensite morphologies are similar to the microstructure of 12%Cr steel observed by Pryds and Huang [20]. Nevertheless, more secondary sawteeth and less secondary sideplates are found in Fig. 3b than those in Fig. 5a. Martensite of 12%Cr stainless steel in HTHAZ with only Nb stabilization reticularly distributes along ferrite grain boundaries. Fig. 5b shows that martensite of steel F in the shape of a net distrib-

Table 1
Chemical compositions of steels tested (wt.%, balance Fe).

Steel code	C	N	Si	Mn	Cr	Ni	Nb	Ti	FF
A	0.011	0.010	0.39	0.99	12.10	1.00	0.00	0.00	7.62
B	0.034	0.013	0.3	1.64	11.46	0.78	0.00	0.33	7.62
C	0.026	0.011	0.28	1.61	11.56	0.79	0.00	0.33	8.02
D	0.014	0.006	0.37	1.47	11.22	0.98	0.07	0.25	8.08
E	0.013	0.010	0.34	1.37	11.50	0.93	0.00	0.26	8.24
F	0.012	0.008	0.35	1.11	12.07	0.98	0.28	0.00	8.35
G	0.010	0.008	0.35	1.14	11.27	0.93	0.49	0.00	8.61
H	0.014	0.009	0.30	1.60	11.60	0.78	0.00	0.33	8.80
I	0.004	0.009	0.33	1.59	11.49	0.76	0.00	0.32	9.29
J	0.012	0.006	0.20	1.50	11.02	0.96	0.00	0.59	9.38
K	0.015	0.011	0.12	1.92	11.11	0.97	0.57	0.52	9.51
L	0.013	0.008	0.25	1.53	11.15	0.98	0.32	0.45	9.71
M	0.008	0.006	0.54	1.06	11.92	0.61	0.075	0.00	10.32
N	0.012	0.007	0.47	1.13	11.77	0.52	0.05	0.11	10.57